FAILURE PREDICTION IN PLASTIC BALL GRID ARRAY ELECTRONIC PACKAGING

Meng-Kao Yeh[1] and Kuo-Ching Chang[2]

Department of Power Mechanical Engineering
National Tsing Hua University
Hsinchu 30043 Taiwan ROC

ABSTRACT

As the electronic and information industry booms in the recent years, traditional electronic packaging technology is no longer sufficient. High density and high performance, lighter, thinner and smaller electronic packages are continuously under development. With a high I/O number, good electronic performance, Plastic Ball Grid Array (PBGA) package has been among the mainstream. However, the assembly of PBGA may fail by the so-called 'popcorn phenomenon' when under humid and heated condition for a long time.

In this paper, the PBGA system equation was derived from the Fourier's heat transfer equation and the Fick's moisture diffusion equation. By applying the finite element method, the deformation and hygrothermal stress distribution for PBGA can be obtained after calculating the temperature and moisture distribution. Owing to the composites nature of electronic packaging, Tasi-Hill failure criteria was modified to predict the failure at the interface around the die and die pad. The parameters, such as the chip size, the adhesive thickness, the die pad size and the thickness of the molding compound, were varied to assess their effects on the failure of PBGA. Proper package parameters of PBGA can prevent its failure at interfaces and furthermore, to improve the reliability of electronic packaging.

INTRODUCTION

The electronic packaging industry has been under development toward high density and high performance, lighter, thinner and smaller in the recent years. With a high I/O number, good electronic performance, high mechanical strength and a lower price, Plastic Ball Grid Array (PBGA) package has been among the mainstream. However, the assembly of PBGA may fail by the so-called 'popcorn phenomenon' when under humid and heated condition for a long time to absorb moisture and to permeate inward simultaneously. When PBGA package is under solder reflow process without any pre-treatment to remove the moisture, the hygrothermal stress at interfaces is induced due to the mismatch of the coefficient of thermal expansion (CTE) and the expansion of moisture within the package. If the hygrothermal stress reaches a critical value, interfacial failure occurs, and may be accompanied eventually by the cracking of the epoxy molding compound (EMC).

The EMC and substrate BT of PBGA are constituted by resin, which absorbs moisture under general environment. The permeability of moisture inside PBGA depends on the temperature and humidity during the packaging of PBGA (Liu, 1993). The moisture content absorbed by EMC and BT depends on their moisture diffusivity, package geometry and the moisture exposure condition (Tay and Lin, 1996), which will influence the reliability of PBGA. During solder reflow at about $221\,^{o}C$, the hygrothermal stress is induced and the package is destroyed when its value exceeds the mechanical strength of the material (Ahn and Kwon, 1995). Usually, there exist some local flaws caused by the crack propagating from the lower and upper edge of the die pad, and from the upper edge of chip after encapsulation and surface mounting process (Lee and Earmme, 1996). The thermal stress, induced from the CTE mismatch between interfaces, causes failure when its value exceeds the adhesion strength of interfaces (Tilgner et al., 1994; Liu et al., 1997; Sauber et al., 1994). Delamination is one of the most important damage modes and may be located at weak interfaces between different materials (Sauber et al., 1994).

The process of popcorn phenomenon in the electronic package includes the moisture absorption, the initiation of delamination failure, the expansion of moisture and the cracking of package. Ahn and Kwon (1995) investigated the delamination damage of package caused by the expansion of moisture at the interface between the chip and die pad. Tay and Lin (1996) studied the delamination under the die pad. Kuo et al. (1994) found that moving evaporation fronts may cause higher stress and delamination at the corner of the interface. Gannamani and Pecht (1996) performed an experimental study of popcorning in plastic encapsulated microcircuits for the verification of theoretical analysis. Yeh and Mung (1998) analyzed the moisture distribution and the hygrothermal stress inside PBGA. Krishna et al. (1995) assumed the epoxy molding compound to be viscoelastic and implemented finite element analysis to obtain temperature and moisture distributions on electronic packaging.

---

[1] Professor, author for correspondence.
[2] Graduate student

This paper uses the finite element method to obtain the hygrothermal stress caused by the moisture and temperature in the PBGA package. The locations of the higher stress inside PBGA, especially at interfaces, were examined. Owing to the composites nature of electronic packaging, Tasi-Hill failure criteria was modified to predict the failure at interfaces between different materials. Proper choice of the package parameters and dimensions can prevent the occurrence of failure at interfaces between different materials and can improve the reliability of electronic packaging.

FINITE ELEMENT ANALYSIS

The structure of plastic ball grid array electronic packaging, as shown in Figure 1, consists of epoxy, die, die pad, substrate, and solder ball. In this paper, the analysis includes (a) heat transfer (b) moisture diffusion (c) hygrothermal stress and (d) failure criterion.

Heat Transfer Analysis

The environmental temperature changes with time in the solder reflow process; therefore, the transient temperature was analyzed for the PBGA packaging. For homogeneous and isotropic materials, the heat transfer coefficient $\kappa_x = \kappa_y = \kappa_z = \kappa$, and the two-dimensional Fourier equation in Cartesian coordinate can be expressed as (Bejan, 1993)

$$\frac{\partial}{\partial x}\left(\kappa\frac{\partial T}{\partial x}\right)+\frac{\partial}{\partial y}\left(\kappa\frac{\partial T}{\partial y}\right)+Q=c_p\rho\dot{T} \qquad (1)$$

where T is temperature, c_p is specific heat, ρ is density, Q is the heat source per unit volume.

The environmental temperature T_0 is assumed on the boundary. Assuming no heat convection, the two-dimensional heat transfer equation can be derived from the following functional by finite element method (Cook et al., 1989).

$$\Pi=\int_V(\tfrac{1}{2}\underline{T}_g^T[\kappa]\underline{T}_g-QT+\rho c_p\dot{T}T)dv \qquad (2)$$

The plane-strain eight-node elements, one degree of freedom per node, are chosen in the analysis. The temperature T within the element can be interpolated from nodal temperature $\underline{T}_e$.

$$T=[N]\underline{T}_e \quad , \quad \underline{T}_g=[B]\underline{T}_e \qquad (3)$$

where $[N]$ is the interpolation matrix consisted from element shape functions; and $[B]=\underline{\partial}_t[N]$ is a matrix consisted of the derivatives of shape functions. From the principle of minimum total potential energy, the global finite element matrix equation is obtained

$$[K]\underline{T}+[C]\dot{T}=0 \qquad (4)$$

where

$$[K]=\Sigma[k],\ [k]=\int_{V_e}[B]^T[\kappa][B]dv \qquad (5a)$$

$$[C]=\sum[c],\ [c]=\int_{s_e}[N]^T c_p\rho[N]dv \qquad (5b)$$

When calculating the field temperature, we assume that $\underline{T}_n$ and $\underline{T}_{n+1}$ are the field temperatures at time t and t+ Δt ; Δt is time increment. According to the generalized trapezoidal rule (Cook et al., 1989)

$$\underline{T}_{n+1}=\underline{T}_n+\left\{(1-\beta)\dot{\underline{T}}_n+\beta\dot{\underline{T}}_{n+1}\right\}\Delta t \qquad (6)$$

where β is an integration factor. From equations (4) and (6)

$$\left\{\frac{1}{\Delta t}[C]+\beta[K]\right\}\underline{T}_{n+1}=\left\{\frac{1}{\Delta t}[C]-(1-\beta)[K]\right\}\underline{T}_n \qquad (7)$$

The initial temperature of PBGA package is assumed to be at room temperature. The field temperature distribution $\underline{T}_{n+1}$ can be obtained from $\underline{T}_n$ using equation (7). The filed temperature at each following time step can be obtained by similar fashion.

When integrating in time axis, the value of Δt is related to the integration factor β (Cook et al., 1989). The system is unconditionally stable for $0.5 \leqq \beta \leqq 1$. The central difference method (β =0.5) is used in this analysis.

Moisture Diffusion Analysis

For homogeneous and isotropic materials, the moisture diffusion coefficient $D_x = D_y = D_z = D_m$. The Fick's equation for two-dimensional moisture diffusion is

$$\frac{\partial}{\partial x}\left(D_m\frac{\partial M}{\partial x}\right)+\frac{\partial}{\partial y}\left(D_m\frac{\partial M}{\partial y}\right)=\dot{M} \qquad (8)$$

where M is the moisture; $\dot{M}$ is the time rate of moisture. The moisture M_0 is specified on the boundary. The two-dimensional finite element equation for moisture diffusion can be obtained similar to the heat transfer analysis. From the principle of minimum total potential energy, the global finite element matrix equation is

$$[D_m]\underline{M}+[C_m]\dot{\underline{M}}=0 \qquad (9)$$

The initial moisture within the package is usually assumed

zero. Similar to the calculation procedure in heat transfer analysis, the moisture $\underline{M}_n$ and $\underline{M}_{n+1}$ are separated by the properly chosen Δt and are obtained using central difference method (β =0.5).

Hygrothermal Stress Analysis

The strain increments can be obtained by multiplying the temperature and moisture with the material thermal expansion and moisture diffusion coefficients.

$$\underline{\varepsilon}_t = \int_{T_1}^{T_2} \alpha_t dT = \alpha_t \Delta T \tag{10}$$

where $\underline{\varepsilon}_t$ is the thermal strain; α_t is thermal expansion coefficient; T_1 and T_2 are temperatures at two steps.

$$\underline{\varepsilon}_m = \int_{M_1}^{M_2} \beta_m dM = \beta_m \Delta M \tag{11}$$

where $\underline{\varepsilon}_m$ is the moisture-induced strain; β_m is moisture diffusion coefficient; M_1 and M_2 are moisture at two steps.

In analysis, the initial strain increment can be expressed as the sum of the thermal strain $\underline{\varepsilon}_t$ and moisture-induced strain $\underline{\varepsilon}_m$.

$$\underline{\varepsilon}_i = \underline{\varepsilon}_t + \underline{\varepsilon}_m \tag{12}$$

The external load vector can be obtained from the initial strain increment. In this paper, the eight-node plane element with two degrees of freedom was used in hygrothermal analysis. The total strain $\underline{\varepsilon}_T$ can be calculated from conventional finite element method used in solid mechanics. The mechanical strain $\underline{\varepsilon}$ can be found as

$$\underline{\varepsilon} = \underline{\varepsilon}_T - \underline{\varepsilon}_t - \underline{\varepsilon}_m \tag{13}$$

The hygrothermal stress $\underline{\sigma}$ can be found from the mechanical strain $\underline{\varepsilon}$.

$$\underline{\sigma} = [E]\ \underline{\varepsilon} \tag{14}$$

After calculating the hygrothermal stress, the interfaces in PBGA are checked for failure according to the failure criterion.

Failure Criterion

Failures in PBGA are mainly due to stress reaching a critical value at interfaces between different materials. For PBGA package, the failures at interfaces are mainly determined from the peel stress $\underline{\sigma}_y$ and the shear stress $\underline{\tau}_{xy}$. The Tsai-Hill failure criterion can be properly modified as (Mei and Liu, 1995)

$$\sqrt{\left(\frac{\underline{\sigma}_y}{\underline{\sigma}_y^f}\right)^2 + \left(\frac{\underline{\tau}_{xy}}{\underline{\tau}_{xy}^f}\right)^2} = f_d \tag{15}$$

where $\underline{\sigma}_y^f$ is the critical peel stress; $\underline{\tau}_{xy}^f$ is the critical shear stress; f_d is the failure index. The interfaces fail when $f_d \geqq 1$.

RESULT AND DISCUSSION

The depopulated 1.27-mm pitch peripherial pad PBGA was analyzed by the finite element method to simulate the JEDEC test process (1995). The Level 1 test standard was chosen. The PBGA was placed in a chamber with 85 °C /85% for 168 hours. During the solder reflow, the temperature increased at 6 °C per second up to 221 °C and stays for 20 seconds. Figure 1 shows the schematic cross-section of PBGA sample. Owing to the symmetry of PBGA, only the right half of PBGA is analyzed for computational efficiency. Figure 2 shows the cross-sectional dimensions of PBGA and the material properties are listed in Table 1.

Moisture Distribution

According to JEDEC (1995) Level 1 moisture test standard, the PBGA was placed in a chamber of 85 °C 85% for 168 hours. Figure 3 shows the mesh, 693 elements and 2256 nodes, used in the moisture analysis by the finite element method. Figure 4 shows the analytical moisture distribution of PBGA after 4, 32, 96, and 168 hours, respectively. According to Figure 4, the moisture diffused from the environment through EMC downward and BT upward to PBGA. The diffusion coefficient of EMC is about 5 times that of BT; therefore, EMC saturated faster to the environment moisture. Since the die and die pad absorbed no water, the moisture reached die attach around the die and die pad after 16 hours. From Figure 4, after 168 hours, EMC and BT reached saturation state and die attach 92% of environmental moisture; therefore, the moisture had influential effects on PBGA during the solder reflow for temperatures above 100 °C.

Temperature Distribution

According to JEDEC (1995) temperature test standard, during solder reflow process, the temperature of PBGA increases from room temperature (17 °C) to 125 °C at 6 °C per second and stays at 125 °C for 20 seconds. Then the temperature increases to 185 °C at 6 °C per second and stays at 185 °C for 120 seconds. The temperature continues to increase to 221 °C at 6 °C per second and stays at 221 °C for 20 seconds. Finally, the temperature of PBGA decreases to room temperature at 6 °C

per second.

Figure 5 shows the mesh, 842 elements and 2701 nodes, used in thermal analysis by the finite element method. Figure 6 shows the PBGA reached external temperature at 221 ^{o}C .

Hygrothermal Stress Analysis

If the initial states of PBGA are assumed: relative humility 0%, room temperature 17 ^{o}C , and zero internal stress, the hygrothermal stresses between interfaces of PBGA are calculated during solder reflow process for the temperature of 221 ^{o}C . The boundary conditions are shown in Figure 7. The top node on the axis of symmetry is hinged. The mesh used in the finite element analysis is shown in Figure 5. As the moisture increased with time, the moisture induced stress at interfaces of the die and die pad due to the mismatch of moisture diffusion coefficient resulting from absorbing no water by the die and die pad. The thermal stress resulted from thermal expansion coefficient mismatch at interfaces between different materials. The moisture-induced stress and the thermal stress were added to obtain hygrothermal stress.

To study the effects of PBGA dimension change on the hygrothermal stresses at interfaces, the dimensions of PBGA are varied and listed in Table 2 for analysis. Interface failure is mainly due to peel stress and shear stress, the allowable peel stress and allowable shear stress at interfaces are listed in Table 3.

Interface between EMC and Die

To study the effect of dimension change of EMC and die on the hygrothermal stress, the dimensions of EMC and die are varied as shown in Table 2 for cases 1, 2, 3, 4 and 11. The analytical hygrothermal stresses at interface between EMC and die are shown in Figure 8 for peel and shear stresses. As can be seen in the figure, the peel stress increases for thicker die and decreases for thinner die and thicker EMC. For the longer EMC or BT, PBGA doesn't fail due to peel stress or shear stress since f_d <1.

Interface between Die and Die Attach

To study the effect of dimension change of the die and die attach on the hygrothermal stress, the dimensions of die and die attach are varied as shown in Table 2 for cases 1, 2, 3, 6 and 7. The analytical hygrothermal stresses at interface between the die and die attach are shown in Figure 9 for peel and shear stresses. From figure 9(b), the shear stresses in cases 3 and 7 reached the critical value of failure at interface. For the thinner die, the peel stress increases near corner and shear stress decreases, but no failure occurs since f_d <1. For the thicker die, shear stress increases to cause f_d >1 and interface fails, though peel stress decreases at corner. For the thicker die attach, the peel stress increases in the compression side at corner and shear stress decreases; thus, the interface is so compressed to prevent failure. For the longer die attach, though the peel stress decreases at interface corner, the shear stress increases so much that f_d >1, and PBGA fails. Therefore, proper choices of thicker die attach and thinner die can prevent interface failure between the die and die attach.

Interface between EMC and Die Pad

To study the effect of dimension change of EMC and die pad on the hygrothermal stress, the dimensions of die and die attach are varied as shown in Table 2 for cases 1, 8, 10 and 11. The analytical hygrothermal stresses at interface between EMC and die pad are shown in Figure 10 for peel and shear stresses. The peel and shear stresses exceed the value to cause failure at the interface corner for all cases due to weak bonding between EMC and the die pad. For the thicker die pad, both the peel and shear stresses decrease at the interface corner. For the longer die pad or thicker EMC, both the peel and shear stresses increase and failure readily occurs. Properly increasing the thickness of die pad can reduce the interface stresses, but the effort is limited and failure may occur. If the bonding strength between EMC and die pad can be increased, interface failure can be prevented effectively. Table 4 shows the results obtained from failure prediction for all cases studied.

During solder reflow, temperature control is critical. Higher temperature can result in higher hygrothermal stresses. Figure 11 shows the analytical results of the peel and shear stresses at the interface between the die and die attach for $221\,^{0}C$, $245\,^{0}C$ and $269\,^{0}C$. As the temperature exceeds $221\,^{0}C$, failure occurs at interface between the die and die attach; therefore, proper control of temperature during solder reflow can prevent interface failure.

CONCLUSIONS

The hygrothermal stress of PBGA electronic packaging was calculated according to environmental changes of moisture and temperature. The failure criterion modified from Tsai-Hill failure criterion was used to check the failure at interfaces of PBGA. The following conclusions can be made.

1. BT has relatively high reliability in moisture environment due to lower moisture diffusion coefficient than EMC's. The saturation of moisture diffuses mainly in the vertical direction.

2. During solder reflow process, failure occurs only at the interface between EMC and the die pad. Owing to weak interface between EMC and die pad, dimension change of EMC and die pad can't prevent failure.

3. Dimension change of EMC and die doesn't cause failure at the interface between EMC and die.

4. At interface between the die and die attach, the stress is at critical state of failure; properly increasing the thickness of die attach and decreasing die thickness can prevent failure at interface. Failure usually occurs at corners of interfaces.

5. Above 221 ^{o}C , failure may occur at the interface between the die and die attach; temperature should be controlled properly

during solder reflow.

ACKNOWLEDGEMENTS

This work was supported by the National Science Council, Taiwan, the Republic of China through grant NSC87-2212-E007-007. The support from National Center for High-performance Computing by providing supercomputer Cray J916 is greatly acknowledged. The authors would also like to thank Professor Kuo-Ning Chiang in our department for valuable discussion and providing an earlier version of computer program for stress analysis.

REFERENCES

Ahn, S. H. and Kwon, Y. S., 1995, "Popcorn Phenomena in a Ball Grid Array Package," *IEEE Transactions on Components, Packaging, and Manufacturing Technology*, Part B, Vol. 18, No. 3, pp. 491-495.

Bejan, A., 1993, *Heat Transfer*, Wiley, New York.

Chiang, K. N., 1997, "Electronic Packaging and Computational Mechanics," News of the Society of Theoretical and Applied Mechanics, the Republic of China, Vol. 81, pp. 1-13. (in Chinese)

Choi, Y. T. and Hu, Y. C., 1998, "Analysis of Popcorn Phenomenon of PBGA by Computer Simulation," Industrial Materials, Vol. 141, pp. 145-152. (in Chinese)

Cook, R. D., Malkus, D. S. and Plesha, M. E., 1989, *Concepts and Applications of Finite Element Analysis*, 3rd ed., Ch. 16, Wiley, New York.

Gannamani, R. and Pecht, M., 1996, "An Experimental Study of Popcorning in Plastic Encapsulated Microcircuits," *IEEE Transactions on Components, Packaging, and Manufacturing Technology*, Part A, Vol. 19, No. 2, pp. 194-201.

JEDEC, JESD22-A1113-A, 1995, "Test Method A113-A Preconditioning of Plastic Surface Mount Devices Prior to Reliability Testing," JEDEC Standard, Electronic Industries Association, Arlington, VA, pp. 1-5.

Krishna, A., Harper, B. D. and Lee, J. K., 1995, "Finite Element Viscoelastic Analysis of Temperature and Moisture Effects in Electronic Packaging," *Journal of Electronic Packaging*, ASME, Vol. 117, pp. 192-200.

Kuo, A. Y., Nguyen, L. T. and Chen, K. L., 1994, "Effects of Moving Evaporation Fronts in Package Popcorning," ASME Winter Annual Meeting, Chicago, IL, November 6-11.

Lau, J. H. and Chen, K. L., 1997, "Thermal and Mechanical Evaluations of a Cost-effective Plastic Ball Grid Array Package," Journal of Electronic Packaging, Vol. 119, pp. 208-212.

Lee, H. and Earmme, Y. Y., 1996, "A Fracture Mechanics Analysis of the Effects of Material Properties and Geometries of Components on Various Types of Package Cracks," *IEEE Transactions on Components, Packaging, and Manufacturing Technology*, Part A, Vol. 19, No. 2, pp. 168-177.

Liu, S., 1993, "Debonding and Cracking of Microlaminates Due to Mechanical and Hygrothermal Loads for Plastic Packaging," *6th Symposium on Structural Analysis in Microelectronics and Fiber Optics*, EEP-Vol. 7, ASME WAM, pp. 1-11, Nov. 28-Dec. 3, New Orleans, Louisiana.

Liu, S., Zhu, J., Zou, D. and Benson, J., 1997, "Study of Delaminated Plastic Packages by High Temperature Moir e′ and Finite Element Method," *IEEE Transactions on Components, Packaging, and Manufacturing Technology*, Part A, Vol. 20, No. 4, pp. 505-512.

Mei, Y. H. and Liu, S., 1995, "An Investigation to Popcorning Mechanisms for IC Plastic Packages: Defect Initiation," *Application of Fracture Mechanics in Electronic Packaging and Materials*, ASME, EEP-Vol. 11/MD-Vol. 64, pp. 85-97.

Minges, M. L. et al., 1989, "Packaging," *Electronic Materials Handbook*, Vol.1, ASM International, Materials Park, OH.

Sauber, J., Lee, L., Hsu, S. and Hongsmatip, T., 1994, "Fracture Properties of Molding Compound Materials for IC Plastic Packaging," *IEEE Transactions on Components, Packaging, and Manufacturing Technology*, Part A, Vol. 17, No. 4, pp. 533-541.

Tay, A. A. O. and Lin, T., 1996, "Moisture Diffusion and Heat Transfer in Plastic IC Packages," *IEEE Transactions on Components, Packaging, and Manufacturing Technology*, Part A, Vol. 19, No. 2, pp. 186-193.

Tilgner, R., Alpern, P., Baumann, J., Pfannschmidt, G. and Selig, O., 1994, "Changing States of Delamination Between Molding Compound and Chip Surface: A Challenge for Scanning Acoustic Microscopy," *IEEE Transactions on Components, Packaging, and Manufacturing Technology*, Part B, Vol. 17, No. 3, pp. 442-448.

Voth, T. E. and Bergman, T. L., 1996, "Ball Grid Array Thermomechanical Response During Reflow Assembly," *Journal of Electronic Packaging*, Vol. 118, pp. 214-222.

Yeh, M. K. and Mung, Y. L., 1998, "Hygrothermal Stress Analysis of Plastic Ball Grid Array Electronic Packaging," Proceedings of the 15th National Conference on Mechanical Engineering, the Chinese Society of Mechanical Engineers, Tainan, Taiwan, R.O.C., Solid Mechanics and Design Volume, pp. 97-104. (in Chinese)

Yi, S., Goh, J. S. and Yang, J. C., 1997, "Residual Stresses in Plastic IC Packages During Surface Mounting Process Preceded by Moisture Soaking Test," *IEEE Transactions on Components, Packaging, and Manufacturing Technology*, Part B, Vol. 20, No. 3, pp. 247-255.

Table 1 Material properties of PBGA

Constant/Material	EMC	Die	Die Attach	Die Pad	BT	Solder Ball
E (Gpa)	0.64[a]	158.62[b]	6.21[b]	119.3[c]	17.4[b]	31.03[b]
$\alpha .10^{-6}$ (/ °C)	17.1[a] (T ≤ 160 °C) 71.4[a] (T > 160 °C)	3[b]	50[b]	16.9[c]	16[d] (x,z) 72[d] (y)	25[b]
$\beta .10^{-5}$ (/%)	4[a]	0	4[a]	0	4[a]	0
ν	0.3[b]	0.21[b]	0.3[b]	0.34[c]	0.28[b]	0.4[b]
K(w/m °C)	0.67[a]	153[a]	4.5[c]	196.6[c]	0.3[a]	50[f]
C_p (J/kg °C)	1884[a]	703[a]	703[c]	400[c]	1570[e]	150[f]
ρ (kg/ m^3)	1820[a]	2330[a]	3800[c]	8920[c]	1800[e]	8520[f]
D_m (mm^2 / s)	3.4×10^{-6}[a]	0	60×10^{-6}[g]	0	0.7×10^{-6}[g]	0

a: (Yi et al., 1997) b: (Choi and Hu, 1998) c: (Lau and Chen, 1997) d: (Chiang, 1997) e: (Voth and Bergman, 1996) f: (Minges et al., 1989) g: (Liu, 1993)

Table 2 Different dimensions used in analysis for PBGA

	EMC	Die	Die Attach	Die Pad	BT	Remark
Case 1	12*1.16	4.1*0.3	4.1*0.06	5.6*0.06	13.5*0.54	Original Dimension
Case 2	12*1.16	4.1*0.2	4.1*0.06	5.6*0.06	13.5*0.54	e-0.1
Case 3	12*1.16	4.1*0.4	4.1*0.06	5.6*0.06	13.5*0.54	e+0.1
Case 4	13.5*1.16	4.1*0.3	4.1*0.06	5.6*0.06	15*0.54	a+0.5 d+0.5
Case 5	10.5*1.16	4.1*0.3	4.1*0.06	5.6*0.06	12*0.84	c+0.3
Case 6	12*1.16	4.1*0.3	4.1*0.1	5.6*0.06	13.5*0.54	f+0.04
Case 7	12*1.16	4.1*0.3	5.4*0.06	5.6*0.06	13.5*0.54	h+1.3
Case 8	12*1.16	4.1*0.3	4.1*0.06	6.6*0.06	13.5*0.54	i+1
Case 9	12*1.16	4.1*0.3	4.1*0.06	7.6*0.06	13.5*0.54	i-1.5
Case 10	12*1.16	4.1*0.3	4.1*0.06	5.6*0.1	13.5*0.54	g+0.04
Case 11	12*1.66	4.1*0.3	4.1*0.06	5.6*0.06	13.5*0.54	b+0.5

Unit : mm

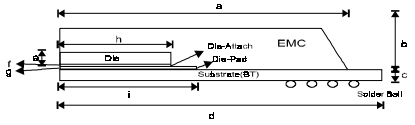

Table 3 Allowable failure stresses at three interfaces

Interface	Allowable Peel Stress (MPa)	Allowable Shear Stress(MPa)
EMC/Die	68.556	68.556
Die/Die Attach	68.556	68.556
EMC/Die Pad	3.567	3.567

Source: (Choi and Hu, 1998)

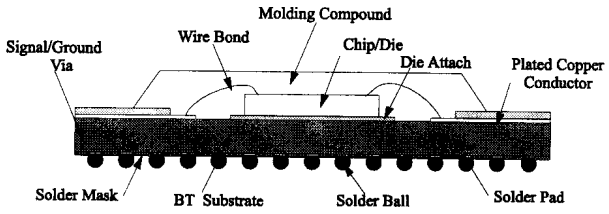

Fig.1 Schematic of plastic ball grid array packaging

Table 4 Failure predictions at three interfaces

	EMC/Die	Die/Die Attach	EMC/Die Pad
Case1	✔	✔	✘
Case2	✔	✔	✘
Case3	✔	✘	✘
Case4	✔	✔	✘
Case5	✔	✔	✘
Case6	✔	✔	✘
Case7	✔	✘	✘
Case8	✔	✘	✘
Case9	✔	✔	✘
Case10	✔	✔	✘
Case11	✔	✘	✘

✔ no failure ✘ failure

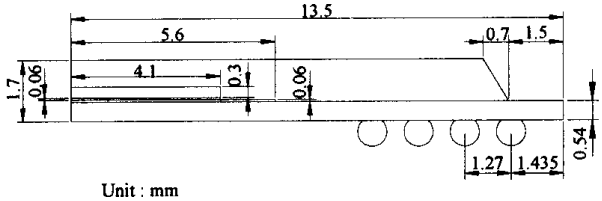

Unit : mm

Fig.2 Cross-sectional dimension of PBGA

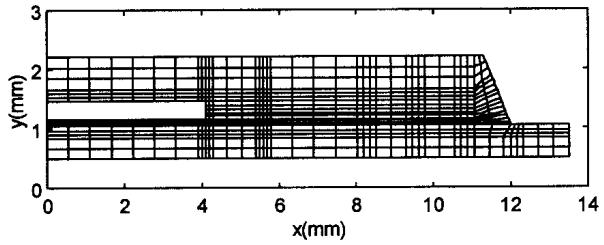

Fig.3 Finite element mesh of PBGA for moisture analysis (693 elements and 2256 nodes)

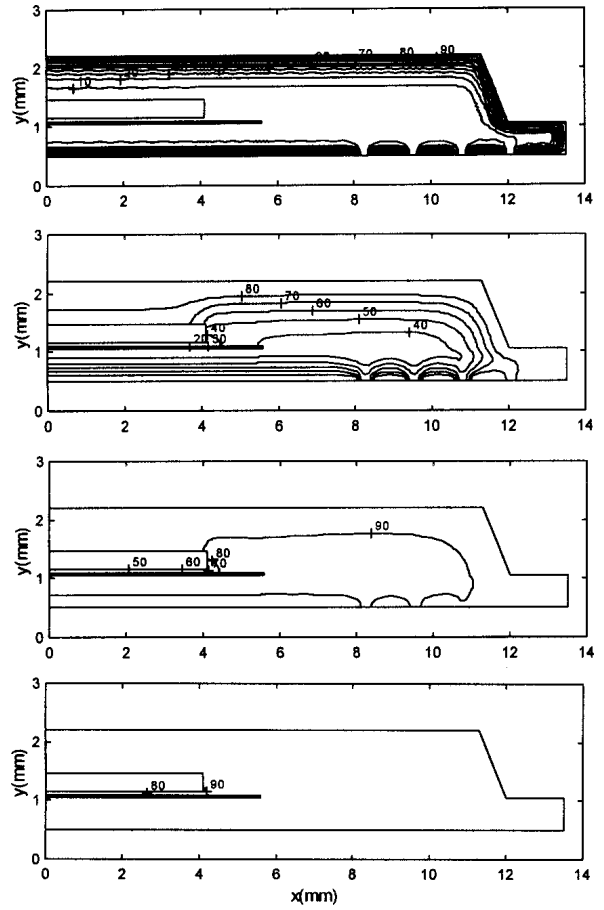

Fig. 4. Moisture distribution of PBGA after 4, 32, 96, 168 hours

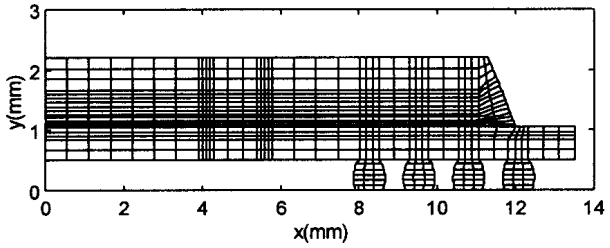

Fig.5 Finite element mesh of PBGA for thermal analysis (842 elements and 2701 nodes)

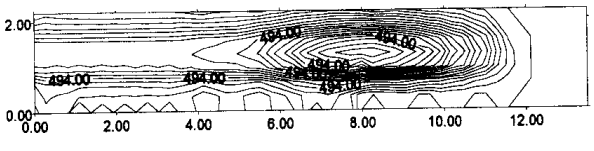

Fig.6 Analytical temperature distribution at 221°C (unit: °K)

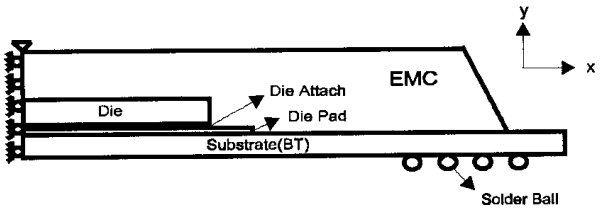

Fig.7 Schematic of boundary conditions of PBGA

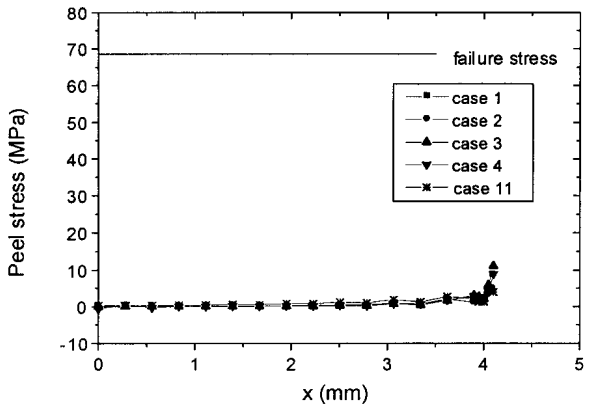

Fig. 8(a)

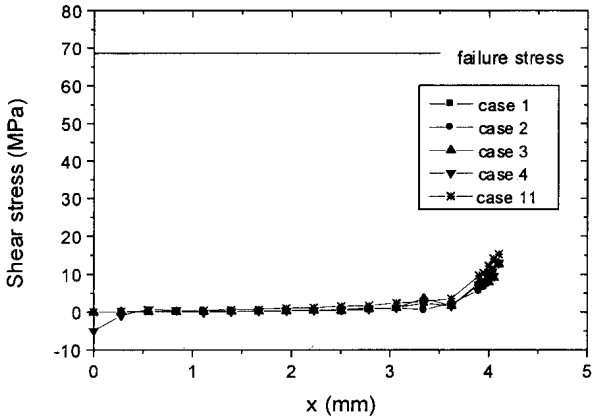

Fig. 8(b)

Fig.8 (a) Peel stress (b) shear stress at interface between EMC and the die

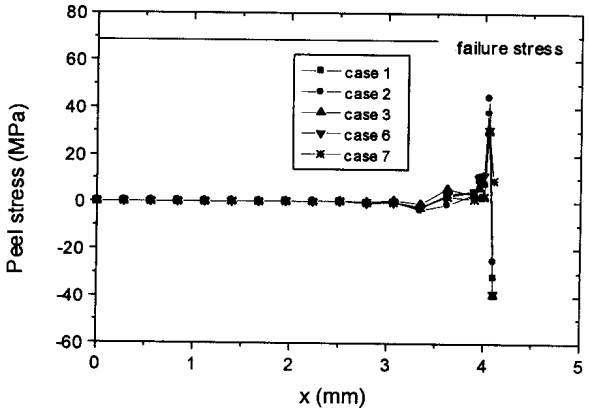

Fig. 9(a)

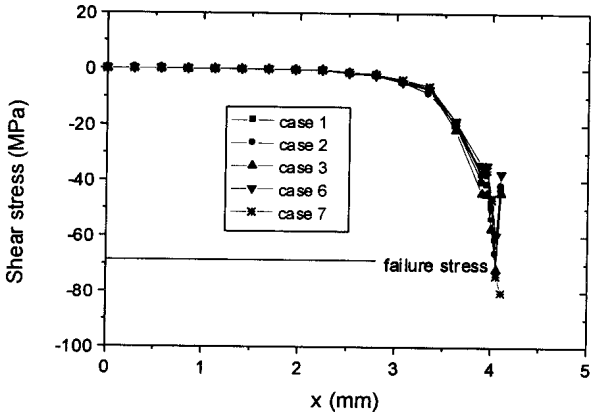

Fig. 9(b)

Fig.9 (a) Peel stress (b) shear stress at interface between the die and die attach

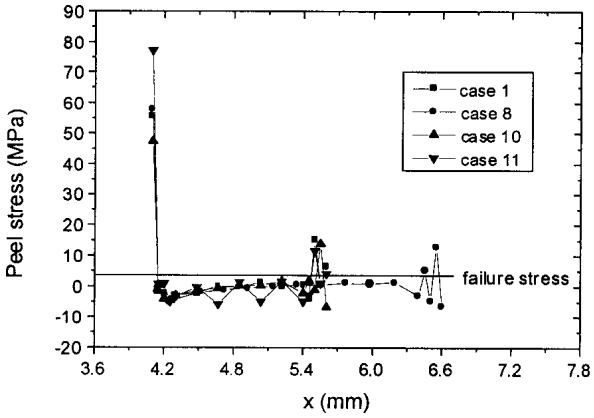

Fig. 10(a)

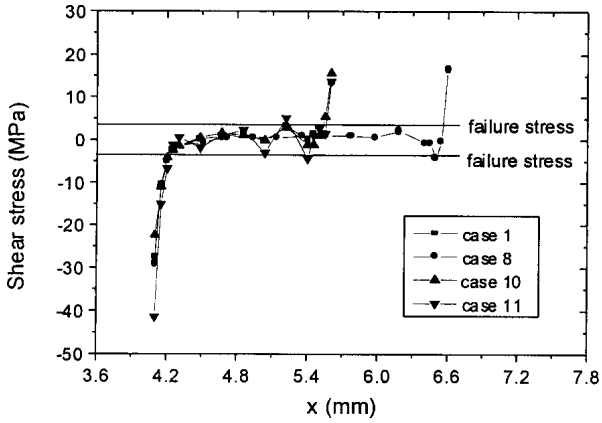

Fig. 10(b)

Fig.10 (a) Peel stress (b) shear stress at interface between EMC and die pad

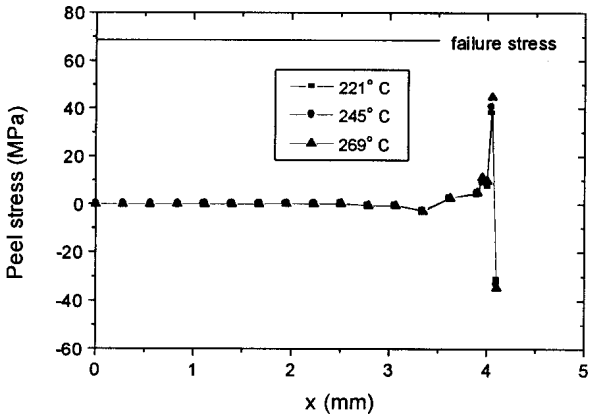

Fig. 11(a)

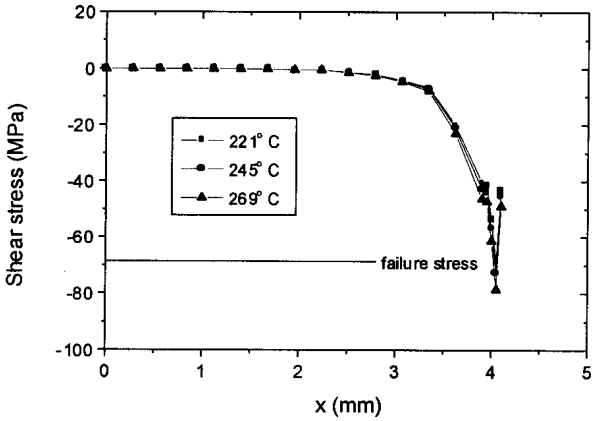

Fig. 11(b)

Fig.11 (a) Peel stress (b) shear stress at interface between the die and die attach at different temperature